Qualitative and quantitative assessment of water sorption in natural fibres using ATR-FTIR spectroscopy

Amandine Célino, Olivier Gonçalves, Frédéric Jacquemin, Sylvain Fréour

1
2
3
Qualitative and quantitative assessment of water sorption in natural fibres using ATR-FTIR spectroscopy

4 A. Célino[1]*, O. Gonçalves [2] F. Jacquemin[1], S. Fréour[1]

5

6

7 [1] Institut de Recherche en Génie Civil et Mécanique, UMR CNRS 6183, 37 Boulevard de
8 l'Université, 44602 Saint-Nazaire Cedex, France,
9 [2] GEPEA, UMR CNRS 6144, 37 Boulevard de l'Université, 44602 Saint-Nazaire Cedex,
10 France

11

12 *Corresponding author: Amandine Célino

13 GeM, UMR CNRS 6183

14 37 Boulevard de l'Université, BP 406

15 44602 Saint-Nazaire Cedex

16 Telephone number: +33240172625

17 Fax number: +33240172618

18 E-mail address: amandine.celino@univ-nantes.fr

19

20 **Abstract**

21 In the field of composite materials, natural fibres appear to be a viable replacement for glass
22 fibres. However, in humid conditions, strong hydrophilic behavior of such materials can lead
23 to their structural modification. Then, understanding moisture sorption mechanisms in these
24 materials is an important issue for their efficient use . In this work, the water sorption on three
25 natural fibres (flax, hemp and sisal) was studied using Fourier Transformed InfraRed
26 spectroscopy. The spectral informations allowed both qualitative and quantitative analysis of
27 the moisture absorption mechanisms. The main chemical functions involved in the water
28 sorption phenomenon were identified. The absolute water content of the fibres was also
29 determined by using a Partial Least Square Regression (PLS-R) approach. Moreover, typical
30 sorption isotherm curves described by Park model were fitted as well as water diffusion
31 kinetics These last applications confirmed the validity of the FTIR spectra based predictive
32 models.

33
34

35 **Keywords***: natural fibres, water sorption, Fourier Transformed InfraRed spectroscopy,*
36 *Partial Least Square Regression, diffusion kinetics*
37
38

39 **1. Introduction**

40 Nowadays, natural fibres are considered to be a good alternative for glass fibres replacement
41 in the purpose of composite material reinforcement (particularly in automotive manufacturing
42 or sport and leisure sector) (Bledzki & Gassan, 1999; Suddell & Evans, 2005). These fibres

43 present a better environmental impact than glass fibres (recyclability, biodegradability) as
44 well as higher specific mechanical properties because of their low density. However, their
45 pronounced hydrophilic behavior -due to their particular structure- leads to high level of
46 moisture absorption in wet environments (Célino, Fréour, Jacquemin, & Casari, 2013). This
47 results in the structural modification of the fibres and an evolution of their mechanical
48 properties together with the composites in which they are fitted in (Dakhal, Zhan, &
49 Richardson, 2007; Placet, Cisse, & Boubakar, 2012; Symington, Banks, David, & Pethrick,
50 2009). Thereby, the understanding of these moisture absorption mechanisms is of great
51 interest to get a better control of such new biomaterials.
52
53 Generally, one of the most important factors controlling the water diffusion phenomenon in
54 polymeric materials is the molecular interaction occurring between the diffusing compound
55 and the substrate. The diffusion phenomenon is subjected to the ability of the polymer
56 molecular sites to establish hydrogen bonds with the water molecules. Spectroscopic
57 techniques such as Nuclear Magnetic Resonance (NMR), dielectric or Fourier Transform
58 Infra-Red spectroscopy (FTIR) have been proved to be well adapted to study this
59 phenomenon since they allow to characterize molecular interactions involving potential
60 sorption sites for water (Mijovic & Zhang, 2003; Popineau, Rondeau-Mouro, Suplice-Gaillet
61 & Martin, 2005). Among these approaches, FTIR spectroscopy has been widely used to study
62 water transport in polymer and particularly to study the water sorbed into epoxy resins
63 (Cotugno, Larobina, Mensitieri, Musto & Ragosta, 2001; Feng, Berger, & Douglas, 2004;
64 Fieldson & Barbari, 1993; Musto, Ragosta, & Mascia, 2000). Indeed, this technique provides
65 attractive features: i.e. the very high sampling rate, the sensitivity, the accuracy of the
66 quantitative analysis and the informations at the molecular level contained in the vibrational
67 spectra. Moreover, the development of Attenuated Total Reflectance FTIR spectroscopy
68 (ATR-FTIR) encouraged and facilitated the use of this non-invasive technique directly onto
69 solid materials (Chalmers & Dent, 1997).
70
71 On pure cellulosic polymers, the potential sorption sites for water were determined to be
72 hydroxyl and carboxyl groups which are particularly easily detected in FTIR spectroscopy
73 (Berthold, Olsson, & Salmén, 1998). However, few studies have been performed to
74 characterize water sorption by FTIR directly on raw lignocellulosic fibres. (Laity & Hay,
75 2000) demonstrated that it was possible to reproduce water sorption kinetics by recording
76 infrared spectra in reflexion mode on cellophane. More recently, (Olsson & Salmén, 2004)
77 examined the association of water on pulp paper using FTIR spectra acquired in transmission
78 mode. Their results indicated the existence of characteristic bands affected by water.
79 Moreover they determined a linear relationship between the absorbance of those bands and
80 the water content, using a univariate approach. This last work was of particular importance
81 since it highlighted major features helping the understanding of chemical groups involved in
82 water diffusion in pulp paper. However both approaches, based on univariate analysis of
83 FTIR signal failed to properly reproduce the sorption isotherms.
84
85 The aim of this work is the use of FTIR as an experimental tool to investigate the water
86 sorption onto raw plant fibres, known to be good candidates for the reinforcement of

2

87   composite materials (i.e. flax, hemp and sisal). First FTIR spectral signature of each fibre was
88   investigated in order to describe the molecular effect of the water sorption mechanisms.
89   Secondly, a multivariate model linking water sorption and the whole FTIR spectra was
90   developed using partial least square regression (PLS-R). Finally this model was applied for
91   the accurate monitoring of the water diffusion in the tested biomaterials.
92
93

94   **2. Materials and methods**

95   *2.1 Materials*

96   Among the disposable plant fibres, hemp, flax, and sisal fibres were chosen because they
97   presented the best mechanical properties regarding the replacement of glass fibres for the
98   purpose of reinforcing the polymeric matrix (Summerscales, Dyssanayake, Virk & Hall,
99   2010; Wambua, Ivens, & Verpoest, 2003,). In our study, the bundle of the model fibres was
100   investigated. Bundle of fibres are extracted from the stem (flax and hemp) or the leaf (sisal) of
101   the plant. They are composed of about ten elementary fibres linked together by a pectic
102   cement (i.e. the middle lamella). Their section is in the order of a few millimeters.
103

104   *2.2 Moisture sorption protocol*

105   First, all thefibre samples tested were dried in desiccators containing silicate gel for 48 hours
106   before controlled moisture sorption treatment. Then, samples were placed in different
107   hygroscopic conditions in a climatic chamber (supplied by Climats and assisted by Spiral 3
108   software) in order to get samples with different water content. The relative humidities tested
109   were 30, 50, 60, 75, 85 and 97 % at room temperature. Experimental sorption isotherms and
110   sorption kinetics were obtained by periodically weighting the samples. Dynamic Vapour
111   Sorption apparatus could also been used to plot sorption isotherms with more accuracy as
112   demonstrated by (Bessadok et al., 2009 or Xie et al., 2011). But in our case, gravimetric
113   measurement provided necessary results. Data were read to 0.01 mg on a precision balance
114   (Sartorius – MC1 Analytic AC210P). The equilibrium moisture content Ms is considered to
115   be reached when the mass is stable according to relation (1).

$$M_W (\%) = \frac{M(t) - M_0}{M_0} \times 100 \qquad (1)$$

116   where M_0 is the initial weight of the bulk specimens before moisture sorption (dry
117   conditions) and M(t) is the weight of the specimen at time t.
118

119   *2.3 Infrared spectroscopic investigations*

120   *2.3.1 ATR-FTIR spectra acquisition*

121   Infrared spectra were recorded in reflection mode directly on the single reflexion diamond
122   crystal of the ATR accessory loaded with bundles of the three fibres presented in section 2.1.
123   The Bruker tensor 27 FTIR spectrometer equipped with the ATR platinum module, with a
124   deuterated triglycine sulphate detector RT-DLaTGS and the OPUSv7.0.122 software (Bruker
125   Optics, Germany) was set up with the following parameters. The spectral resolution was fixed

3

126 to 1 cm^{-1}, the number of scans to 32, the selected spectral range between 4000 and 400 cm^{-1}.

127 The penetration depth in the fibres was 0.4 µm at 4000 cm^{-1} and 2.7 µm at 600 cm^{-1} according

128 to equation (2) relating penetration depth (dp) to wavelength.

$$dp = \frac{\lambda}{2 \Pi n_1 \sqrt{\sin^2 \theta - (n_2/n_1)^2}} \qquad (2)$$

129 Where λ is the infrared wavelength, n_1, the refractive index of the internal reflexion element

130 (IRE), n_2 the refractive index of the substrate and θ the angle of incidence of the IR beam

131 (Griffith & Haseth, 2007). In our case $n_1 = 2.41$, $n_2 = 1.5$ for the fibres assimilated as polymer,

132 $\theta = 40°$, and $\lambda = 4000\text{-}600$ cm^{-1}).

133 Background spectra were collected using the same instrument settings as those employed for

134 the samples and was performed against air. Spectra were recorded for 10 replicates per fibre

135 sample.

136

137 *2.3.2 ATR-FTIR spectra acquisition in kinetic mode*

138 For the monitoring of water diffusion, time dependent ATR-FTIR spectra were acquired

139 every 2 minutes in ambient conditions during drying of a saturated fibre sample. Each tested

140 fibres were systematically placed in a relative humidity atmosphere of 95 % before the

141 measurement. Recorded spectra were directly treated by Partial Least Square regression

142 (section 2.3.4) in order to determine the water content and to plot the drying kinetics of the

143 tested fibres. Then, the results were compared with the kinetics obtained by the gravimetric

144 measurements. For the gravimetric measurements, the samples were placed on a precision

145 balance (0.01 mg) during the drying step and data were collected every 2 minutes.

146

147 *2.3.3 ATR-FTIR spectra preprocessing*

148 All the spectra were recorded to the background spectra. For the PLS-R model calibration

149 and validation the raw spectra were used since OPUS v 7.0.122 software was set up to

150 manage spectral corrections automatically, according to the value of its optimization criteria.

151 For the Kruskal Wallis analysis the raw spectra were corrected for ambient CO_2 only and

152 smoothed. For the multivariate analysis, the raw spectra were corrected for ambient CO_2,

153 smoothed and a second derivative calculation was also performed. All these treatments were

154 achieved using integrated functions of (Bruker Optics, Germany)

155 *2.3.4 Qualitative Multivariate analysis of ATR-FTIR spectra*

156 Pre-processed spectra or pre-processed second derivative spectra were exported as text files

157 for file format modification on Microsoft Excel v14.0.0 or statistical treatment on R 2.15.2.

158 Second derivative spectra were systematically used to improve the infrared band resolution

159 and thus enhance the discrimination of vibrators contributing to the shape of raw FTIR spectra

160 (Mecozzi, Pietroletti, & Tornambe, 2011). The spectral data were centered and scaled (mean

161 subtracted and divided by standard deviation) to minimize the unit range influence before

162 performing unsupervised multivariate analysis (Principal Component Analysis (PCA) and

163 Hierarchical Clustering on Principal Components (HC-PC)) using the factominer R package

164 (Lê, Josse & Husson, 2008). The number of classes was determined without a priori by firstly

4

165 using the unsupervised multivariate analysis (i.e. PCA). A refined assessment of the clusters
166 was then performed using a Partial Least Square Discriminant Analysis (PLS-DA), conducted
167 on all the wave numbers stemming from the ATR-FTIR spectra. This multivariate approach
168 was used in order to enhance the formation of clusters by using a model of class prediction
169 (for review see Wold, Sjöström, & Eriksson, 2001). The quality of the prediction was
170 characterized by two parameters, $R^2(Y)$ (goodness of the fit) and Q^2 (predictive capability of
171 the model). The clustering capabilities of the PLS-DA model were considered as satisfactory
172 with both $R^2(Y)$ and Q^2 values superior to 0.5 (Westerhuis et al., 2008). The generation of the
173 PLS-DA models was performed in two steps: first the calibration step ($R^2(Y)$ and Q^2), second
174 the validation step named also the cross validation step ($R^2(Y)$int and Q^2int). For the cross
175 validation step, (Westerhuis et al., 2008) latest study indicated clearly that it was important to
176 notice that even with negative Q^2int values, it was still possible to obtain clear separation
177 between classes. The PLS-DA analysis was conducted using the web server analysis pipeline
178 Metaboanalyst 2.0, dedicated to metabolomic data exploitation (Xia, Mandal, Sinenikov,
179 Broadhurst, & Wishart, 2012). For this supervised multivariate analysis ATR-FTIR spectral
180 data were Log10 [1+x] - transformed and Pareto scaled (divided by the square root of the
181 standard deviation) (Van den Berg, Hoefsloot, Westerhuis, Smilde, & Van Der Werf, 2006).
182 To assess the influence of the water content on the ATR-FTIR spectra of the tested fibres, a
183 Kruskal Wallis Test (non parametric ANOVA) was performed per wave number of the ATR-
184 FTIR raw spectra recorded on a tested fibre for different water contents. As this non
185 parametric version of the ANOVA does not make any assumption on the nature of the
186 underlying distribution (it does not assume the distribution to be normal), it should be less
187 sensitive to the outliers commonly found in FTIR signatures (since the outliers are taken into
188 account). This allowed a better detection of the vibrators impacted by the water uptake (Di
189 Giambattista et al., 2011). P-value beyond significance threshold (0.05) were plotted on raw
190 spectra data in order to visualize impact of water sorption on ATR-FTIR bands.
191
192
193 *2.3.5 Quantitative analysis of ATR-FTIR spectra*

194 There are two steps to obtain PLS-R models: the calibration and the validation. Generally two
195 kinds of validation can be performed: the cross validation and the external validation. Usually
196 the calibration and the cross validation are performed in a single step since identical data set is
197 used to perform calculation.
198
199 *(i) Calibration and cross validation*

200 For the calibration (cross validation) step, the procedure of calculation and selection of the
201 best predictive model was iterative and comprised a loop formed of two steps. Firstly the pre-
202 processed infrared spectra were regressed against the reference value (i.e. for a considered
203 fibre: its water content determined gravimetrically). Secondly a full cross validation of the
204 model was performed by omitting one sample and operating the test in the remaining spectral
205 data set. This procedure allowed finding models with high correlations R^2 and low Root Mean
206 Square Error of Cross-Validation (RMSECV). The infrared data sets used in our study

5

207   comprised 11 samples and 5 replicates per sample, i.e. 55 spectra (ASTM Committee E13,
208   2005).

209   *(ii) External validation*

210   An independent data set was used for the model evaluation (4 samples and 5 replicates per
211   sample, i.e. 20 spectra) in order to obtain highest correlations (i.e. high R^2) and lowest root
212   mean square error of prediction (RMSEP).

213

214   **3. Results and discussion**

215   *3.1 FTIR qualitative analysis of the water uptake effect on the studied fibres*

216   *3.1.1 Each model fibre presented its own FTIR fingerprint*

217   The second derivative spectral data were qualitatively analysed using Partial Least Square
218   Discriminant Analysis (PLS-DA) for each model fibres and for three different relative
219   humidities (RH = 10, 50 and 97 %). On figure 1, results indicate that the three fibres are
220   clustered into three distinct groups, clearly associated to each type of fibre (axis 1). Inside
221   each cluster, it is moreover possible to distinguish subgroups according to relative humidity
222   content (axis 2).
223   The clustering results clearly reveal that each type of fibre could be distinguished according to
224   its FTIR spectrum, exhibiting moreover differences for the three tested relative humidities.
225   Those observations suggest that each fibre presents its own FTIR signature, depending on its
226   proper chemical composition. Indeed, according to the work of Satyanarayana and colleagues
227   (Satyanarayana, Arizaga, & Wypych, 2009) this spectral signature could be directly related to
228   the amount of the constitutive macromolecules (cellulose, hemicelluloses, lignin and pectin)
229   and to the crystallization degree of the cellulose which are both fibre dependent. Moreover,
230   as the chemical make-up and the crystallinity degree of the fibres are known to influence the
231   moisture sorption, the PLS-DA results suggest that each fibre should present its own water
232   diffusion behavior. Taken together all those remarks indicate that the water quantification
233   models should be developed per type of fibres.
234

6
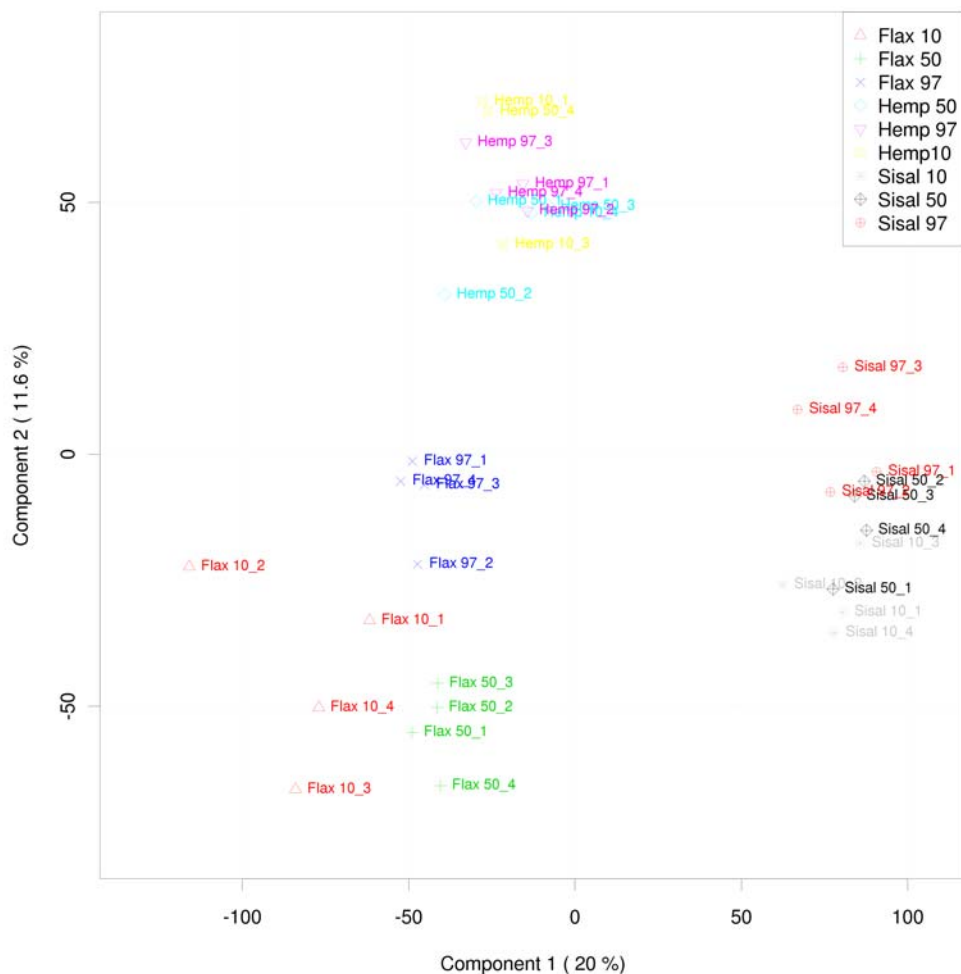
235
236 **Figure 1:** *PLS-DA score plot of second derivative FTIR signatures of the three model fibres*
237 *for three RH conditions.*
238 *The legend in the upright corner details the nature of the model fibre and the values of the*
239 *tested RH % (as suffixes). The classification model used here presented the following*
240 *characteristics i.e. R²(Y) = 0,989 and Q² = 0,869 and was validated using 20 permutations*
241 *(R²(Y)int = 0,555 and Q²int = -0,343).*
242 *3.1.2 Water sorption molecular sites could be identified for the model fibres subjected to*
243 *increasing RH %*

244 The spectral dependence on the water content is illustrated on figure 2. The development of
245 the sisal FTIR spectra by increasing relative humidity and water content has been treated here
246 solely for reason of clarity. Similar results were observed for hemp and flax fibres (data not
247 shown). The results of the Kruskal Wallis analysis performed on each individual wave
248 number of the raw spectra highlight several zones of the sisal FTIR fingerprint that were
249 strongly impacted by the increasing water uptake. It helps the FTIR spectra bands assignation
250 (using table 1) and allows the interpretation of the experimental observations.

251
252 **Table 1:** *Assignment of the main absorption bands in FTIR spectra of sisal, flax and hemp*
253 *fibres. Sisal FTIR data were interpreted according to investigations issued from (Adibi,*

7

254 *Cabrales, & Haigler, 2013; De Rosa, Kenny, Puglia, Santulli, & Sarasini, 2010; Liang &*
255 *Marchessault, 1959; Nelsson & O'Connor, 1964).*
256

Wave number (cm⁻¹)	Assignment
3600-3100	Hydrogen bonded of OH stretching in cellulose and/or hemicelluloses
2935	CH stretching of cellulose and hemicelluloses
2862	CH_2 stretching of cellulose and hemicelluloses
1735	C=O stretching vibration of carboxylic acid in pectin or ester group in hemicelluloses
1635	OH bending vibration characteristic of sorbed water
1595	Aromatic ring in lignin
1502	Aromatic ring in lignin
1425	Carboxylic acid of pectin and COO- vibration
1375	CH bending of cellulose and hemicelluloses
1335 - 1315	CH_2 wagging of cellulose and hemicelluloses
1275	Characteristic peak of lignin
1240	C-O of acetyl in pectin or hemicelluloses
1160	anti-symmetrical deformation of the C-O-C band
1125-895	C-O stretching and ring vibrational modes
895	Characteristic of β-links in cellulose
700-650	O-H out of plane bending

257
258
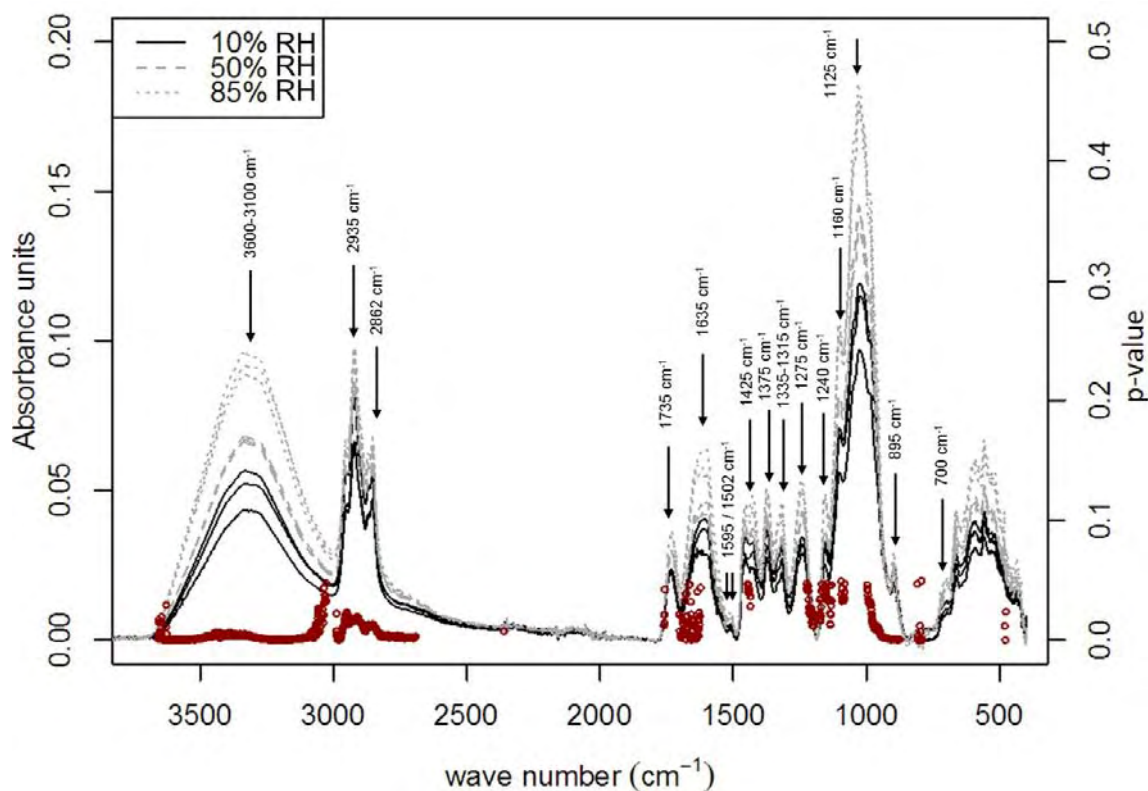
259
260 **Figure 2**: *Infrared spectra bands impacted by increasing relative humidity for sisal fibre.*

8

261 *For clarity, only sisal fibre has been presented and only three relative humidities are shown*
262 *for three replicates (10 %; 50 % and 85 %). p-values scores, indicating significant impact of*
263 *the water uptake on the FTIR bands, were marked using red dots.*
264

265 *(i) Part of the water-fibre interactions could be associated to the formation of hydrogen bonds*
266 *between the water and the hydroxyl groups of the cellulose or hemicelluloses constitutive of*
267 *the raw material.*

268 The broad and unresolved band situated between 3600 and 3000 cm^{-1} was found to be
269 significantly impacted by the increasing relative humidity content. Potential molecular sites of
270 the polymers constituting the studied fibre could be identified here to explain the interactions
271 with the water molecules. Indeed, this band is generally associated to the OH stretching
272 vibrations and hydrogen bonds of hydroxyl groups found in cellulosic materials. However, the
273 absence of clear structured shape makes difficult the assignment of this absorption band
274 (Fengel, 1992; Marchessault, 1962). Recently, (Kondo, 1997) and (Hinterstoisser & Salmèn,
275 1999) helped its resolution by using fitting deconvolution model and DMA-FTIR coupled
276 analysis, respectively. The hydrogen bonds of hydroxyl groups in the 3600-3000 cm^{-1} wave
277 number range were thus associated to general intramolecular and intermolecular hydrogen
278 bonding and to free hydroxyl in cellulose macromolecule. This peak is also representative of
279 the contribution of the free or the bound water linked to the substrate (Cotugno, Mensitieri,
280 Musto, & Sanguigno, 2005; Murphy & Pinho, 1995; Musto et al., 2000). Here it could be the
281 amorphous phase of the cellulose or the hemicelluloses of the material.
282

283 *(ii) The water uptake could be also characterized by the monitoring of the interaction*
284 *between the polymers constituting the raw fibre and the free water.*

285 The interaction of the cellulose or the hemicelluloses molecular sites of sisal, with the free
286 water is also suggested by the significant impact monitored for the FTIR band situated at
287 1635 cm^{-1}. Indeed such modification was already observed in the case of water diffusion and
288 absorption on cellulosic material, and was found to be characteristic of the free water sorbed
289 on studied material (Laity &Hay, 2000; Murphy & Pinho, 1995). The existence of this
290 interaction should be normally reinforced by the presence of a peak situated at approximately
291 700 cm^{-1} and assigned to the out of plane bending of the hydroxyl groups characteristic of the
292 free water molecule. However this last peak is not clearly highlighted by the Kruskal Wallis
293 analysis to be dependent of the water content, bringing therefore uncertainty about the
294 influence of free water contribution monitoring. This lack of characterization could be
295 partially explained by the fact that in spectra recorded in attenuated total reflectance, the
296 definition between 700 cm^{-1} and 400 cm^{-1} could not be as good as in transmission mode,
297 precluding therefore the exploitation of the spectral information situated in this range of wave
298 numbers (Parker & Roy, 1966).
299

300 *(iii) Other molecular sites impacted by the increasing water content could be suggested.*

301 The FTIR bands situated in the wave number interval ranging from 1100 to 700 cm^{-1} were
302 also found to be affected by the water uptake. This signature could be associated to the
303 stretching of the C-O-C group of the polysaccharide components of the studied fibres and

9

304   confirmed the previous observation of Olsson and colleagues (Olsson & Salmén, 2004). The
305   evolution of the peak situated at 1425 cm^{-1}could also be associated to the interaction of the
306   water to the carboxylic acid moiety of the pectin polymer as firstly depicted by Marchessault
307   in his exhaustive study on wood polysaccharides infrared spectra (Marchessault, 1962).
308   Surprisingly, according to the Kruskal Wallis p values assignment, the CH stretching bands
309   situated at 2935 and 2900 cm^{-1} were found to be significantly impacted by the water uptake.
310   This is difficult to interpret, since no clear chemical explanation could be envisaged. Several
311   hypotheses could however bring elements of understanding. It could be inherent to the
312   material which is known to be subject to chemical intrinsic variability or be assigned to non-
313   specific experimental variation. Indeed, tests have been performed on different raw fibres for
314   the identical humidities and it effectively highlighted differences in this specific range of
315   wave numbers (data not shown). The way the spectra were processing could also bring
316   elements of explanation. Indeed they were analyzed with almost the same preprocessing
317   treatment than the one used for the PLS-R model generation. In particularly they were not
318   baseline corrected. The shoulder of the OH stretching vibration band clearly shifted up the
319   whole CH bands when the amount of water increases in the sample -whereas no significant
320   increase of the area was monitored (data not shown). This should perturb the Kruskal Wallis
321   test in this particular zone, since it was performed per wave numbers and not per groups of
322   wave numbers –i.e. a band. The combined use of a smoothing function or of moving average
323   performed onto the p values results could enhance the pertinence of the Kruskal Wallis test.
324   These last observations should be carefully considered in the forthcoming multivariate
325   analysis interpretations.
326
327   *3.1.3 Summary*

328   The results presented above showed that it was possible to discriminate the type of fibre thru
329   its ATR-FTIR second derivative signature using a PLS analysis. Moreover, results revealed
330   that the whole fibre infrared spectra were impacted by the moisture changes. These features
331   strongly suggest that to monitor accurately the water diffusion in the tested biomaterials, a
332   multivariate approach should be used. Indeed, it should improve the water content prediction
333   compared to a univariate approach since the spectral information linked with an increasing
334   water content is visible on the whole spectrum.

335

336   *3.2 FTIR quantitative analysis of the water content of the studied fibres*

337   *3.2.1 It was possible to predict the water uptake of every tested fibre by developing material*
338   *dependent PLS-R models*

339   The absolute water content of the tested fibres was determined by using a Partial Least Square
340   Regression (PLS-R) approach. For each kind of fibre, the MIR spectra were used in the range
341   from 4000 cm^{-1} to 400 cm^{-1} with the corresponding water uptake measured gravimetrically, to
342   calculate multiple PLS-R models and to perform their validation. The models calculated from
343   the information contained in the spectral regions situated between 3600 cm^{-1} to 3200 cm^{-1} and
344   around 1650 cm^{-1} were selected preferentially since they were associated to the main regions
345   characteristics of the interaction between the water and the polymers constituting each
346   studied fibres (3.1). Other regions were not excluded since they could be associated to the

10

347   material intrinsic variability (e.g. around 2900 cm^{-1}). The automatic pre-processing
348   treatments, the spectral regions and the quality indicators (i.e. the cross-validation and the test
349   set validation results) used to calculate the PLS-R models are summarized in the table 2. The
350   spectral regions selected without a priori are in very good agreement with the observations
351   performed in 3.1, especially for the sisal fibre which presents a wave number range
352   distribution correlated to the three main components known to interact with the water
353   molecules. Moreover, the estimation of the errors associated to the predictive models,
354   highlights their pertinence since the RMSECV and RMSEP are very low ($\leq$ to 1). The
355   average number of PLS components is inferior to 7 and the average coefficient of
356   determination greater than 96 %, confirming the quality of the selected models The
357   significance of these parameters has been well described in FitzPatrick and colleagues latest
358   works (FitzPatrick, Champagne & Cunningham, 2012). The figure 3 illustrates the cross-
359   validation and the test set validation results obtained for the sisal fibre. The dispersion
360   diagrams, displaying the relationships between predictive moisture content obtained by PLS-
361   R quantitative model and gravimetric measurements show a very good correlation ($R^2 > 98$).
362
363

11

364
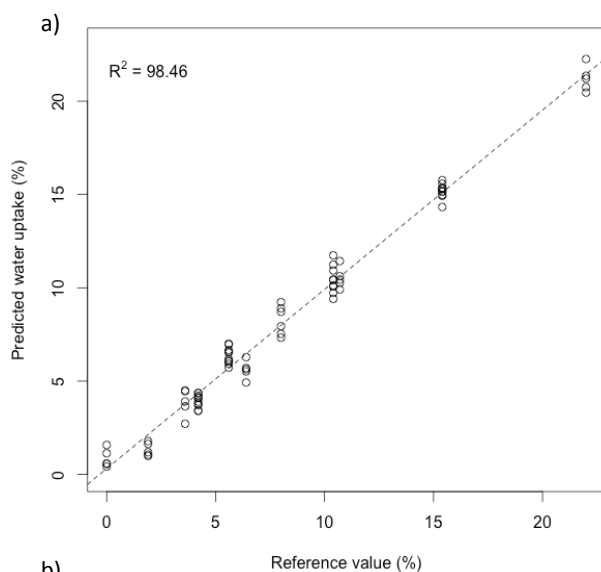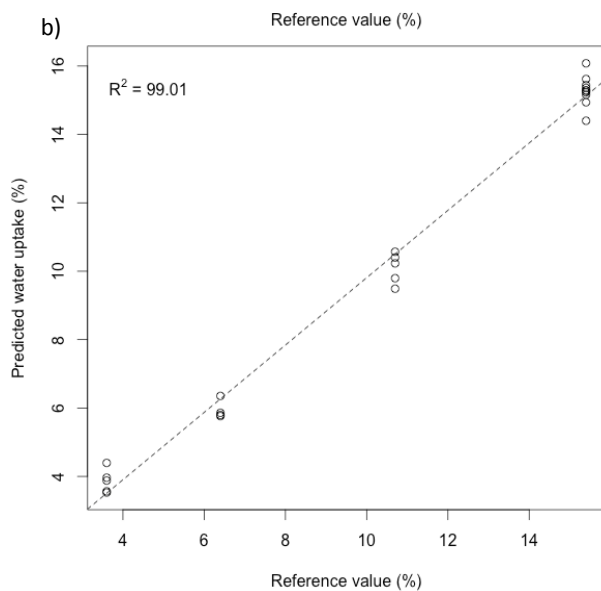
365

366

367 **Figure 3***: Cross-validation (a) and test set validation (b) results of water uptake prediction*
368 *for sisal fibre.*
369 *The PLS-R predictions of the water content obtained with the FTIR approach were compared*
370 *here to the gravimetric measurements. The water uptake is expressed in % of the dry weight*
371 *of the sisal fibre. The coefficients of determination (%) of the regression lines (indicated in*
372 *dotted lines) are indicated in the upper left corner.*

373

374

375

376

377

378

379

380

381

382

12

383   **Table 2**: *PLS-R quality parameters for cross and test set validation for the models selected*
384   *for the three studied fibres.*
385   *RMSECV stands for Root Mean Square Error of Cross Validation. RMSEP stands for Root*
386   *Mean Square Error of Prediction. R² is the coefficient of determination.*
387

		Hemp	Flax	Sisal
	Pre-processing	First derivative	Min/max normalization	Normalization by vector
	Spectral region (cm^{-1})	3998-1119 /760-400	3998-3277 / 2559-2198 / 1839-400	3998-3277 / 1839-1479/ 1120-400
Cross validation	RMSECV	1.14	1.07	0,72
	Number of PLS components	4	9	6
	R² (%)	95.26	94.92	98.46
External validation	RMSEP	0.620	0.843	0,515
	Number of PLS components	5	7	7
	R² (%)	97.90	96.65	99.01

388

389   *3.3 The calculated predictive models were applied to quantify the water sorption phenomenon*
390   *on the three tested fibres*

391   *3.3.1 Monitoring of the sorption isotherm using PLS-R models*

392   The estimation of the water uptake of each studied fibre according to its relative humidity
393   exposition was performed using FTIR spectral information and gravimetric measurements as
394   reference method. FTIR data were interpreted in two ways, one using information arising
395   from one band characteristic of the water sorption (univariate approach) and one exploiting
396   the data of the whole FTIR spectra (multivariate approach: PLS-R model). First, the fibre
397   relative water content was estimated to be solely representative of the absorbance variation of
398   the hydroxyl groups situated in the 3600-3000 cm^{-1} range as already depicted by Olsson &
399   Salmén (2004) (3.1.2). Second, the PLS-R models developed for each studied fibre were used
400   to predict the absolute water uptake taking into account the whole FTIR spectral information.
401   The sorption isotherms present a similar shape for the three studied fibres, whether they were
402   depicted by gravimetric measurements or deduced by FTIR data. The figure 4 illustrates the
403   case of the sisal and indicated that the water content is directly related to the relative
404   humidity by following a sigmoidal relation, as already described by (Alix et al., 2009;
405   Gouanvé, Marais, Bessadok, Langevin & Métayer, 2007). That kind of sorption isotherms are
406   in a good agreement with the Park's model (Park, 1986). This model assumes the association
407   of three mechanisms describing the three parts of the curve (figure 4). It is often used to
408   explain the sorption isotherms of hydrophilic and porous media, as cellulosic fibres (Bessadok
409   et al., 2009).
410   The first part of the curve could be related to Langmuir's mode (RH < 10 %, this mode is not
411   really visible on the figure 4). At these relative humidities, water is sorbed onto specific sites
412   by hydrogen bonding. As discussed in the section 3.1.2 (qualitative analysis of the bands
413   impacted by water) the specific sites could be hydroxyl functions of amorphous cellulose and
414   hemicelluloses or carboxylic function of pectin. When relative humidity increases, there is a

13

415   saturation of these specific sites of sorption. Then, the water concentration increases linearly
416   with relative humidity as Henry's law describes (until RH = 65 %). This behavior could be
417   explained by the porous structure of fibres where water is free to diffuse. The third part is well
418   described by a power function that represents an aggregation phenomenon of water
419   molecules. Indeed, at high relative humidity, water concentration is too important, and water
420   molecules linked together to form clusters.

421   It is important to notice that the prediction arising from the FTIR PLS-R model fits very
422   well the experimental gravimetric measurements ($R^2 > 99$), highlighting the pertinence of the
423   FTIR multivariate approach compared to the FTIR univariate method ($R^2 < 90$).

424
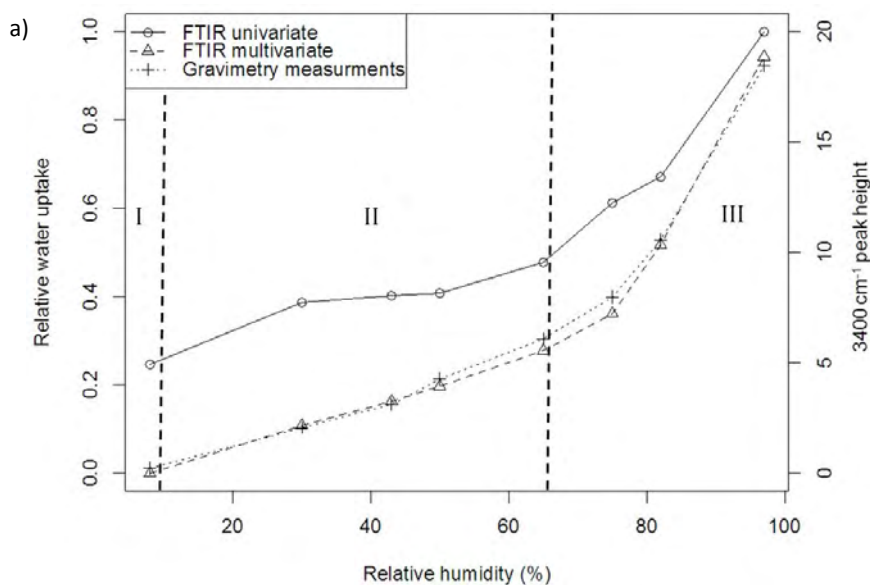
425
426
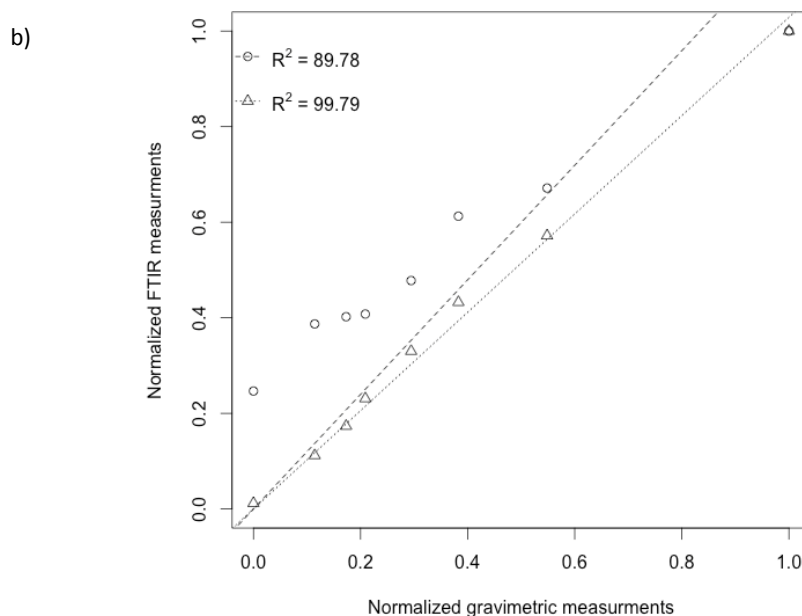
427
428   ***Figure 4****: Comparison of sorption isotherm for sisal fibre using FTIR and gravimetric*
429   *approaches. (a) Sorption isotherm plotted for the sisal fibre according to the measurement*
430   *method (FTIR univariate, FTIR multivariate, gravimetry). (b) Comparison performed between*

14

431   *normalized FTIR measurements and normalized gravimetric reference method measurements*
432   *(FTIR univariate-gravimetry: ○, FTIR multivariate-gravimetry :△). R^2 stands for coefficient*
433   *of determination (%).*
434
435   *3.3.2 Monitoring of the diffusion kinetic using PLS-R models*

436   The desorption kinetics of the water sorbed by the studied fibres were also monitored by
437   exploiting the multivariate FTIR approach. The fibre samples were first aged at RH = 95 %
438   until saturation was reached. Second, FTIR spectra were recorded in kinetic mode during their
439   drying in ambient relative humidity conditions i.e. RH = 45 ± 3 %. FTIR spectral information
440   was treated using the developed PLS-R models for each kind of studied fibres and compared
441   to the gravimetric measurements, systematically performed in parallel. For reason of clarity,
442   the desorption kinetics of sisal fibre is solely represented on figure 5a. FTIR data, predict that
443   after moisture sorption in a wet environment at RH = 95 %, the relative mass gain reached 19
444   %. This value was correlated with our gravimetric measurements and previous works realized
445   on similar materials (Gouanvé et al., 2007; Stamboulis, Baillie & Peijs, 2001). The desorption
446   kinetic   present a sigmoidal shape that could be interpreted as being the consequence of a
447   delay time in the establishment of a water concentration equilibrium at the surface of the
448   studied fibre (similar behaviour was monitored for the others studied fibres (data not shown).
449   At the end of the experiment the initial weight of the fibre was not recovered. A relative mass
450   loss of about 8 %, compared to the initial weight, was observed. Such mass loss could be
451   attributed to the existence of water content in fibres at ambient relative humidity (Baley,
452   Morvan, & Grohens, 2005).
453
454   Our experimental data could be well fitted by the Carter and Kibler model as described in
455   Célino and colleagues previous works (Célino et al., 2013). In this model, the moisture
456   absorption is described quantitatively by assuming that the absorbed moisture consisted of
457   both a mobile (i.e. free water) and a bound phase (i.e. bound water). Molecules of the mobile
458   phase should diffuse spontaneously with a concentration and stress independent diffusion
459   coefficient D_γ, and should be absorbed with a probability per unit time γ at certain molecular
460   sites of the polymer fibre. On the other hand, molecules of the bound phase should be
461   released, becoming thereby mobile, with a probability per unit time β. This assumption was
462   supported by the qualitative FTIR spectral data recorded during the diffusion kinetic (figure
463   5b). Indeed, during the monitoring of the water desorption phenomenon, the main impacted
464   regions (diminishing absorbance) corresponded to the vibration regions of both the free and
465   bound water (3600-3200 cm^{-1}) and the free water uniquely (1635 cm^{-1}) . Those experimental
466   observations strengthen the assumption of the Carter and Kibler model, suggesting that two
467   kind of water population coexisted in the fibres during absorption or desorption. Water should
468   bind to specific sites as hydroxyl or carboxyl functions and free mobile water could diffuse
469   inside the fibre porous structure.
470
471   The curve obtained by gravimetric measurement or determined by the PLS-R model based on
472   ATR-FTIR measurement,   are in a good agreement. A slight slope difference could be
473   however observed during the transient step. This could be attributed to the fact that the two
474   kinetics were not strictly monitored in identical conditions (section 2.3.2). In gravimetric

15

475   measurement, bundle of fibres were free of physical constraints whereas in ATR-FTIR
476   measurements, fibres were pressed above the measurement crystal. The pressure applied by
477   the ATR hammer could accelerate the diffusion of the water from the fibre sample, explaining
478   therefore the observed deviation.
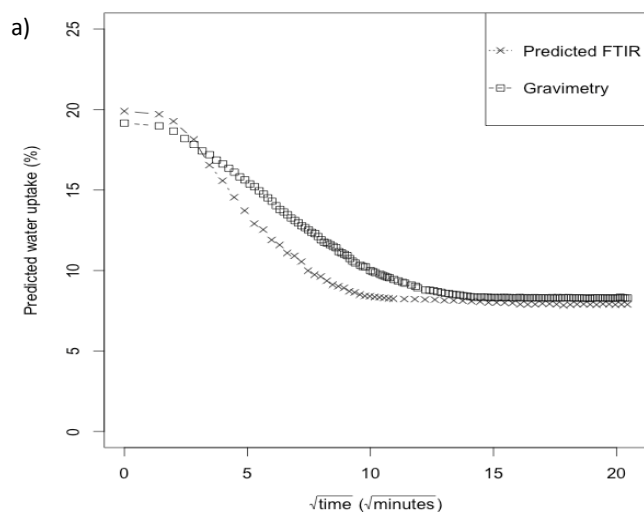
479
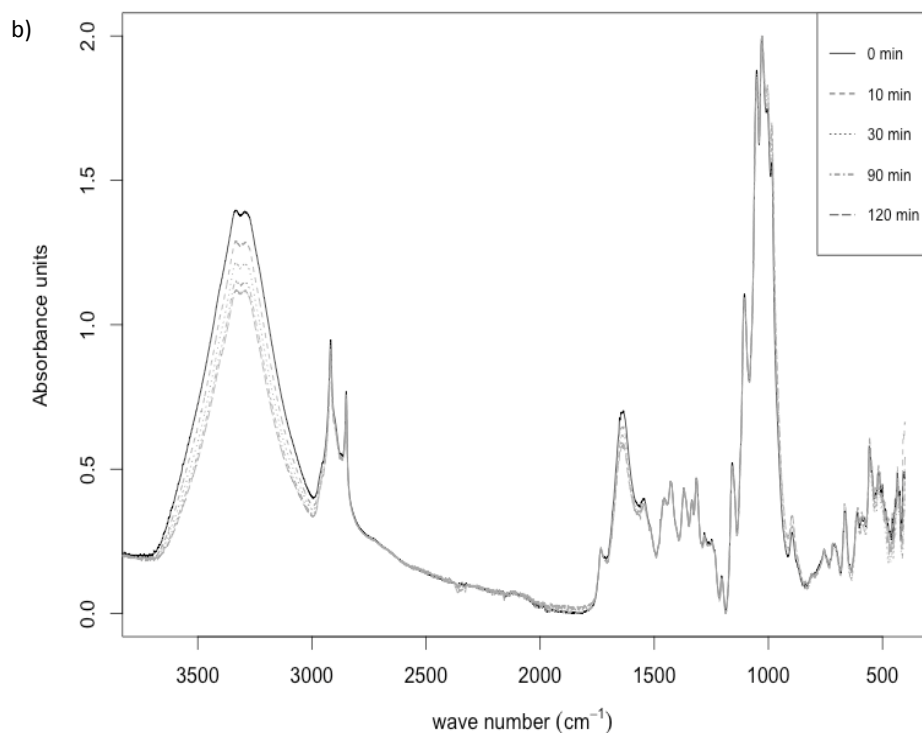
480
481   ***Figure 5:*** *Quantitative and qualitative monitoring of the water diffusion kinetic for the sisal*
482   *fibre. (a) Desorption kinetics monitored by FTIR PLS-R prediction and gravimetric*
483   *approaches. (b) FTIR spectra recorded during kinetic monitoring for time =0, 10, 30, 90 and*
484   *120 min.*
485   **4. Conclusion**

486   In the emerging field of composite biomaterials, natural fibres promise an immense potential
487   of application. However, their strong hygroscopic behavior requires the understanding of the
488   moisture sorption mechanisms. Their water content is also of great importance since it could

16

489 drive the final properties of the composites where they are fitted in. The aim of this work was
490 to develop a quick and easy method based on ATR-FTIR spectroscopy to characterize
491 qualitatively and quantitatively the water sorption phenomenon directly on raw fibres.
492
493 First, our results indicated that it was necessary to develop an approach per fibre since the
494 three tested biomaterials presented their own FTIR signature and therefore their own chemical
495 fingerprint. Hydroxyl and carboxyl molecular sites of the fiber polymer were found to be
496 directly impacted by the water uptake, and confirmed the results observed with less structured
497 cellulosic material (Berthold et al., 1998, Olsson & Salmén, 2004). Second, the FTIR PLS-R
498 models developed for each fibre, in order to quantify their water content, showed very good
499 predictive abilities when compared to the reference method (gravimetric measurements).
500 They were used to monitor accurately sorption isotherms whereas univariate FTIR models
501 could not fit it correctly as depicted by Olsson and colleagues (Olsson & Salmén, 2004). The
502 proposed approach could also supply readily interpretable kinetic data by monitoring
503 continuously the water desorption. The main advantage is the interpretation of kinetics at the
504 molecular level by studying the impacted spectral bands. More detailed analysis
505 (deconvolution of the OH valency band) could lead to the discrimination of the free and the
506 bound water as described in Cotugno and colleagues previous work on an epoxy system
507 (Cotugno et al., 2005).
508
509 Moreover, our results indicated that the information collected at the surface of the fibre could
510 be efficiently correlated to a global method based on volumetric measurements (i.e.
511 gravimetry). The multivariate approach used to characterize the water sorption dynamically or
512 statically could explain the quality of the results and should encourage the use of such a direct
513 and rapid approach for water sorption mechanism study on other cellulosic biomaterials.
514

515 **References:**

516 ASTM Committee E13 on Molecular Spectroscopy and Chromatography. (2005). Standard
517 practices for infrared multivariate quantitative analysis. E 1655-05, 1-29.
518
519 Adibi, N., Cabrales, L., & Haigler, C.H. (2013). Changes in the cell wall and cellulose content
520 of developing cotton fibers investigated by FTIR spectroscopy. *Carbohydrate Polymers. In*
521 *press.*
522
523 Alix, S., Philippe, E., Bessadok, A., Lebrun, L., Morvan, C., & Marais, S. (2009). Effect of
524 chemical treatments on water sorption and mechanical properties of flax fibres. *Bioresource*
525 *and Technology*, *100*, 4742-4749.
526
527 Baley, C., Morvan, C., & Grohens, Y. (2005). Influence of absorbed water on the tensile
528 strength of flax fibers. *Macromolecules Symposium*, *222*, 195-202.
529
530 Berthold, J., Olsson, R.J.O., & Salmén, L. (1998). Water sorption to hydroxyl and carboxylic
531 acid groups in Carboxymethylcellulose (CMC) studied with NIR-spectroscopy. *Cellulose, 5*,
532 280-298.
533

17

534 Bessadok, A., Langevin, D., Gouanvé, F., Chappey, C., Roudesli, S., & Marais, S. (2009).
535 Study of water sorption on modified Agave fibres. *Carbohydrate Polymers, 76*, 74–85.
536
537 Bledzki, A.K., & Gassan, J. (1999). Composites reinforced with cellulose based fibres,
538 *Progress in Polymer Science, 24*, 221–274.
539
540 Célino, A., Fréour, S., Jacquemin, F., & Casari, P. (2013). Characterization and modeling of
541 the moisture diffusion behaviour of natural fibres. *Journal of Applied Polymer Science, In*
542 *press.* DOI: 10.1002/app.39148.
543
544 Chalmers, J.M., & Dent, G. (1997). Industrial Analysis with Vibrational Spectroscopy, RCS.
545
546 Cotugno, S., Larobina, D., Mensitieri, G., Musto, P., & Ragosta, G. (2001). A novel
547 spectroscopic approach to investigate transport processes in polymers: the case of water
548 epoxy system. *Polymer*, *42*, 6431-6438.
549
550 Cotugno, S., Mensitieri, G., Musto, P., & Sanguigno, L. (2005). Molecular interactions in and
551 transport properties of densely cross linked networks: a time resolved FTIR spectroscopy
552 investigation of the epoxy/H2O systems. *Macromolecules, 38*, 801-811.
553
554 De Rosa, I.M., Kenny, J.M., Puglia, D., Santulli, C., & Sarasini, F. (2010). Morphological,
555 thermal and mechanical characterization of okra (Abelmoschus esculentus) fibres as potential
556 reinforcement in polymer composites. *Composite Science and Technology, 70*, 116-122.
557
558 Di Giambattista, L., Pozzi, D., Grimaldi, P., Gaudenzi, S., Morrone, S., & Castellano, A. C.
559 (2011). New marker of tumor cell death revealed by ATR-FTIR spectroscopy. *Analytical and*
560 *Bioanalytical Chemistry, 399*, 2771-2778.
561
562 Dhakal, H.N., Zhang, Z.Y., & Richardson, M.O.W. (2007). Effect of water absorption on the
563 mechanical properties of hemp fibre reinforced unsaturated polyester composites, *Composite*
564 *Science and Technology, 67*, 1674–1683.
565
566 Feng, J., Berger, K.R., & Douglas, E.P. (2004). Water vapor transport in liquid crystalline
567 and non-liquid crystalline epoxies. *Journal of Materials Science, 39*, 3413-3423.
568
569 Fengel, D. (1992). Characterization of Cellulose by Deconvoluting the OH Valency Range in
570 FTIR Spectra. *Holsforshung, 46*, 283-288.
571
572 Fieldson, G.T., & Barbari, T.A. (1993). The use of FTIR-ATR spectroscopy to characterize
573 penetrant diffusion in polymers. *Polymer, 34*, 1146-1153.
574
575 FitzPatrick, M., Champagne, P., & Cunningham, M. (2012). Quantitative determination of
576 cellulose dissolved in 1-ethyl-3-methylimidazolium acetate using partial least squares
577 regression on FTIR spectra. *Carbohydrate Polymers, 87,* 1124-1130.
578
579 Gouanvé, F., Marais, S., Bessadok, A., Langevin, D. &, Métayer, M. (2007). Kinetics of
580 water sorption in flax and PET fibers. *European Polymer Journal, 43*, 586–598.
581
582 Griffiths, P.R., & Haseth, J.A. (2007). Fourier Transformed Infrared Spectrometry (pp.321-
583 329), Second edition. John Wiley & Sons, Inc.

18

584

585   Hinterstoisser, B., & Salmén, L. (1999). Two-dimensional step-scan FTIR: a tool to unravel
586   the OH-valency-range of the spectrum of Cellulose I. *Cellulose 6*, 251-263.

587

588   Kondo, T. (1997). The assignment of IR absorption bands due to free hydroxyl groups in
589   cellulose. *Cellulose, 4,* 281-292.

590

591   Laity, P.R., & Hay, J.N. (2000). Measurement of water diffusion through cellophane using
592   attenuated total reflectance-fourier transform infrared spectroscopy. *Cellulose, 7*, 387-397.

593

594   Liang, C.Y., & Marchessault, R.H. (1959). Infrared spectra of crystalline polysaccharide. I.
595   Hydrogen bonds in native cellulose. *Journal of Applied Polymer Science, 39*, 269-278.

596

597   Lê, S., Josse J., & Husson, F. (2008). FactoMineR: A R Package for Multivariate Analysis.
598   *Journal of Statistical Software, 25*, 1-18.

599

600   Marchessault, R.H. (1962). Application of infra-red spectroscopy to cellulose and wood
601   polysaccharides. *Pure Applied Chemistery, 5*, 107-130.

602

603   Mecozzi, M., Pietroletti, M., & Tornambe, A. (2011). Molecular and structural characteristics
604   in toxic algae cultures of Ostreopsis ovata and Ostreopsis spp. evidenced by FTIR and FTNIR
605   spectroscopy. *Spectrochimica Acta Part A: Molecular and Biomolecular Spectroscopy, 78*,
606   1572-1580.

607

608   Mijovic, J., & Zhang, H. (2003). Local dynamics and molecular origin of polymer network-
609   water interactions as studied by broadband dielectric relaxation spectroscopy, FTIR and
610   molecular simulations. *Macromolecules, 36*, 1279-1288.

611

612   Musto, P., Ragosta, G., & Mascia, L. (2000). Vibrational spectroscopy evidence for the dual
613   nature of water sorbed into epoxy resins. *Chemistery of Material, 12*, 1331-1341.

614

615   Murphy, D., & Pinho, M.N. (1995). An ATR-FTIR study of water in cellulose acetate
616   membranes prepared by phase inversion. *Journal of Membrane Science, 106,* 245-257.

617

618   Nelsson, M.L., & O'Connor, R.T. (1964)**.** Relation of Certain Infrared Bands to Cellulose
619   Crystallinity and Crystal Lattice Type. Part I. Spectra of Lattice Types I, 11, I11 and of
620   Amorphous Cellulose. *Journal of Applied Polymer Science, 8*, 1311-1324.

621

622   Olsson, A.M., & Salmén, L. (2004). The association of water to cellulose and hemicelluloses
623   in paper examined by FTIR spectroscopy. *Carbohydrate Research, 339*, 813-818.

624

625   Park, G. S. (1986). Transport principles: Solution, diffusion and permeation in polymer
626   membranes. In P. M. Bungay et al. (Eds.). Synthetic membranes: Science, engineering and
627   applications (57). Holland: Reidel Pub.

628

629   Parker, F.S. & Roy, A. (1966). Infrared spectra of carbohydrates (700 – 250 cm^{-1}) determined
630   by both Attenuated Total Reflectance and Transmission techniques. *Applied Spectroscopy,*
631   *20*, 384-388.

632

19

633   Placet, V., Cisse, O., & Boubakar, L. (2012). Influence of environmental relative humidity on
634   the tensile and rotational behaviour of hemp fibres. *Journal of Materials Science, 47*, 3435–
635   3446

637   Popineau, S., Rondeau-Mouro, C., Sulpice-Gaillet, C., & Martin E.R.S. (2005). Free/bound
638   water absorption in an epoxy adhesive. *Polymer, 46*, 10733-10740.

640   Satyanarayana, K.G., Arizaga, G.G.C., & Wypych, F. (2009). Biodegradable composites
641   based on lignocellulosic fibers - An overview. *Progress in Polymer Science, 34***,** 982–1021.

643   Stamboulis, A., Baillie, C.A., & Peijs, T. (2001). Effect of environmental conditions on
644   mechanical and physical properties of flax fibres. *Composites Part A*, *32*, 1105-1115.

646   Suddell, B.C., & Evans, W.J. (2005). Natural Fiber Composites in Automotive Applications.
647   In Mohanty, A.K., Misra, M. & Drzal, L.T. (Eds.), Natural Fibers in Biopolymers & Their
648   BioComposites (pp. 231-259). CRC Press.

650   Summerscales, J., Dissanayake, N.P.J., Virk, A.S., & Hall, W. (2010). A review of bast fibres
651   and their composites. Part I-Fibres as reinforcements. *Composites : Part A, 41*, 1329-1335.

653   Symington, M.C., Banks, W.M., David, W.O, & Pethrick, R.A. (2009). Tensile Testing of
654   Cellulose Based Natural Fibers for Structural Composite Applications. *Journal of Composite*
655   *Materials, 43*, 1083-1108.

657   Van den Berg, R. A., Hoefsloot, H. C., Westerhuis, J. A., Smilde, A. K., & Van Der Werf, M.
658   J. (2006). Centering, scaling, and transformations: improving the biological information
659   content of metabolomics data. *BMC Genomics, 7*, 142-153.

661   Wambua, P., Ivens, J., & Verpoest, I. (2003). Natural fibres: can they replace glass in fibre
662   reinforced plastics? *Composite Science Technology, 63*, 1259–1264.

664   Westerhuis, J. A., Hoefsloot, H. C. J., Smit, S., Vis, D. J., Smilde, A. K., Velzen, E. J. J., John
665   P. M., van Duijnhoven, Ferdi A. van Dorsten. (2008). Assessment of PLSDA cross validation.
666   *Metabolomics, 4*, 81-89.

668   Wold, S., Sjöström, M., & Eriksson, L. (2001). PLS-regression: a basic tool of chemometrics.
669   *Chemometrics and Intelligent Laboratory Systems, 58*, 109-130.

670   Xia, J., Mandal, R., Sinelnikov, I.V., Broadhurst, D., & Wishart, D.S. (2012). MetaboAnalyst
671   2.0-a comprehensive server for metabolomic data analysis. *Nucleic Acids Research, 40,* 127-
672   133.

673   Xie, Y., Hill, C.A.S., Jalaludin, Z., Curling, S.F., Anandjiwala, R.D., Norton , A.J. &
674   Newman, G. (2011). The dynamic water vapour sorption behaviour of natural fibres and
675   kinetic analysis using the parallel exponential kinetics model. *Journal of Material Science*,
676   *46*, 479-489.

678   **List of figures**

679   **Figure 1:** PLS-DA score plot of second derivative FTIR signatures of the three model fibres
680   for three RH conditions.

20

681 The legend in the upright corner details the nature of the model fibre and the values of the
682 tested RH % (as suffixes). The classification model used here presented the following
683 characteristics i.e. $R^2(Y) = 0,989$ and $Q^2 = 0,869$ and was validated using 20 permutations
684 $(R^2(Y)int = 0,555$ and $Q^2int = -0,343)$.

685

686 **Figure 2**: Infrared spectra bands impacted by increasing relative humidity for sisal fibre.
687 For clarity, only sisal fibre has been presented and only three relative humidities are shown
688 for three replicates (10 %; 50 % and 85 %). p-values scores, indicating significant impact of
689 the water uptake on the FTIR bands, were marked using red dots.

690

691 **Figure 3**: Cross-validation (a) and test set validation (b) results of water uptake prediction for
692 sisal fibre.
693 The PLS-R predictions of the water content obtained with the FTIR approach were compared
694 here to the gravimetric measurements. The water uptake is expressed in % of the dry weight
695 of the sisal fibre. The coefficients of determination (%) of the regression lines (indicated in
696 dotted lines) are indicated in the upper left corner.

697

698 **Figure 4**: Comparison of sorption isotherm for sisal fibre using FTIR and gravimetric
699 approaches. (a) Sorption isotherm plotted for the sisal fibre according to the measurement
700 method (FTIR univariate, FTIR multivariate, gravimetry). (b) Comparison performed between
701 normalized FTIR measurements and normalized gravimetric reference method measurements
702 (FTIR univariate-gravimetry: ○, FTIR multivariate-gravimetry :△). R^2 stands for coefficient
703 of determination (%).

704

705 **Figure 5:** Quantitative and qualitative monitoring of the water diffusion kinetic for the sisal
706 fibre. (a) Desorption kinetics monitored by FTIR PLS-R prediction and gravimetric
707 approaches. (b) FTIR spectra recorded during kinetic monitoring for time =0, 10, 30, 90 and
708 120 min.

709

710 **List of tables**

711 **Table 1:** Assignment of the main absorption bands in FTIR spectra of sisal, flax and hemp
712 fibres. Sisal FTIR data were interpreted according to investigations issued from (Adibi,
713 Cabrales, & Haigler, 2013; De Rosa, Kenny, Puglia, Santulli, & Sarasini, 2010; Liang &
714 Marchessault, 1959; Nelsson & O'Connor, 1964).

715

716 **Table 2**: PLS-R quality parameters for cross and test set validation for the models selected for
717 the three studied fibres.
718 RMSECV stands for Root Mean Square Error of Cross Validation. RMSEP stands for Root
719 Mean Square Error of Prediction. R^2 is the coefficient of determination.
720

21

720 | HIGHLIGHTS
721

722 - Effect of moisture sorption on plant fibres was investigated by FTIR spectroscopy.
723 - Hydroxyl and carboxyl moieties are specific sites for water sorption.
724 - Partial least squares regression quantified the water content of natural fibres.
725 - Models fitted the sorption isotherms and diffusion kinetics.
726
727
728

22